Heterogeneous Catalysis

DOI: 10.1002/ange.201408754

Thermal Non-Oxidative Aromatization of Light Alkanes Catalyzed by Gallium Nitride**

Lu Li, Xiaoyue Mu, Wenbo Liu, Xianghua Kong, Shizhao Fan, Zetian Mi, and Chao-Jun Li**

Abstract: *The thermal catalytic activity of GaN in non-oxidative alkane dehydroaromatization has been discovered for the first time. The origin of the catalytic activity was studied experimentally and theoretically. Commercially available GaN powders with a wurtzite crystal structure showed superior stability and reactivity for converting light alkanes, including methane, propane, n-butane, n-hexane and cyclohexane into benzene at an elevated temperature with high selectivity. The catalyst is highly robust and can be used repeatedly without noticeable deactivation.*

Benzene, toluene, and xylene, the so-called BTX family, are widely used as basic building blocks for the production of pesticides, polymers, and plastics. However, the traditional methods of producing BTX from thermolysis of naphtha feedstock have encountered challenges because of the rise of oil prices. Therefore, vast and low-cost light alkanes (C_1–C_6 alkanes), such as natural gas (methane) and liquified petroleum gas (propane or butane), are becoming more and more attractive for the production of aromatic hydrocarbons.[1–7] Tremendous attempts have been made for such conversions and several promising catalyst systems have been developed, such as the metal-modified zeolites,[8–11] the pincer-ligated iridium homogeneous complexes,[12] and the lattice-confined single iron sites embedded within a silica matrix.[13] Notably, gallium species in diverse forms turned out to bear remarkable potential for the activation of C–H bonds of light alkanes[14–18] and the selective catalytic reduction (SCR) of nitric oxide by methane.[19] Moreover, the catalytic efficiency for non-oxidative alkane aromatization can be increased significantly by the incorporation of gallium into zeolites.[15,20] However, all reported alkane conversion catalysts to date are limited to metal oxides, which are the most ubiquitous and most extensively investigated inorganic materials. Besides oxides, nitride compounds constitute another important class of heterogeneous catalysts.[21] Very recently, we reported the discovery of photocatalytic conversion of methane on Si-doped GaN nanowires for the first time.[22] However, synthesis of such nanostructured catalysts requires special molecular beam epitaxy techniques under high temperature (ca. 800 to 1000 °C for the growth).[23] In consideration of practical applications, a simple protocol based on easily obtained GaN materials to convert light alkanes into benzene is highly desirable. We hypothesized that the commercialized nondoped GaN powders may possess some unique reactivity towards the thermally catalyzed conversion of methane and other light alkanes. Herein, we wish to report that the easily obtained GaN powders can catalyze the non-oxidative aromatization of short-chain alkanes (C_1–C_6) at elevated temperature with superior thermal stability and catalytic performance [Eq. (1)].

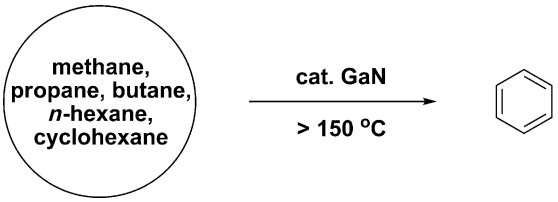

(1)

GaN is an III–V nitride semiconductor (see Figure S1 in the Supporting Information) with a d^{10} electronic configuration. The very high bonding energy (8.9 eV/atom) of the Ga–N bond with a largely ionic component character, makes GaN a thermally and chemically stable material with an ultrahigh melting point (> 2500 °C). No decomposition can be detected up to 1000 °C, even under vacuum.[24] Figure 1a shows the transmission electron microscopy (TEM) image of typical commercialized GaN nanoparticles. Although the morphology of these nanoparticles is not quite uniform, the enlarged TEM images and their corresponding electron diffraction patterns reveal that these GaN nanoparticles possess a regular wurtzite crystal structure (Figures 1b–d), which is the thermodynamically stable phase of GaN. It also shows clearly that most of the exposed surfaces of the GaN nanoparticles are composed of their *c*-planes (0001) and *m*-planes $(1\bar{1}00)$. The overall *m*-plane of GaN is nonpolar since it is composed of equal numbers of Ga and N atoms which are tetrahedrally coordinated with each other, whereas the polar *c*-plane comprises only one type of atom (either Ga or N) which exhibits piezoelectric polarization along the *c*-axis. The

[*] Dr. L. Li, X. Y. Mu, W. B. Liu, Prof. Dr. C.-J. Li
Department of Chemistry and FQRNT Center for Green Chemistry and Catalysis (CCVC), McGill University
801 Sherbrooke Street West, Montreal, QC H3A 0B8 (Canada)
E-mail: cj.li@mcgill.ca
Dr. L. Li, S. Z. Fan, Prof. Dr. Z. T. Mi
Department of Electrical and Computer Engineering, McGill University, 3480 University Street, Montreal, QC H3A 0E9 (Canada)
E-mail: zetian.mi@mcgill.ca
X. H. Kong
Department of Physics, McGill University
3600 rue University, Montréal, QC, H3A 2T8 (Canada)

[**] This work was financially supported by the Canada Research Chair (Tier 1) foundation, NSERC, FQRNT, Canada Foundation for Innovation (CFI), and McGill University.

Supporting information for this article is available on the WWW under http://dx.doi.org/10.1002/anie.201408754.

 © 2014 Wiley-VCH Verlag GmbH & Co. KGaA, Weinheim

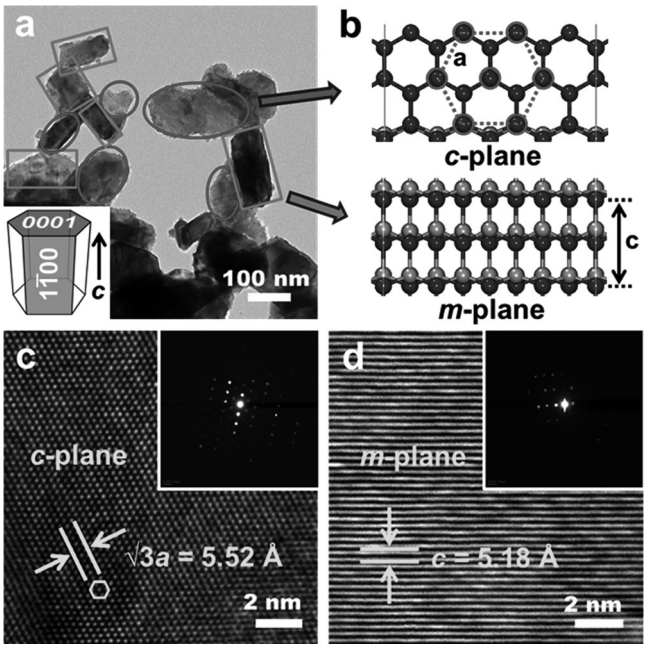

Figure 1. a) TEM image of the GaN nanoparticles with wurtzite structure (the inset). b) Schematic showing the exposed *c*-plane and *m*-plane of GaN nanoparticles indicated in (a). The black and gray spheres represent N and Ga atoms, respectively. c) High-resolution TEM images of the *c*-plane and d) *m*-plane with their corresponding selected area electron diffraction patterns (the insets of 1c and 1d), respectively.

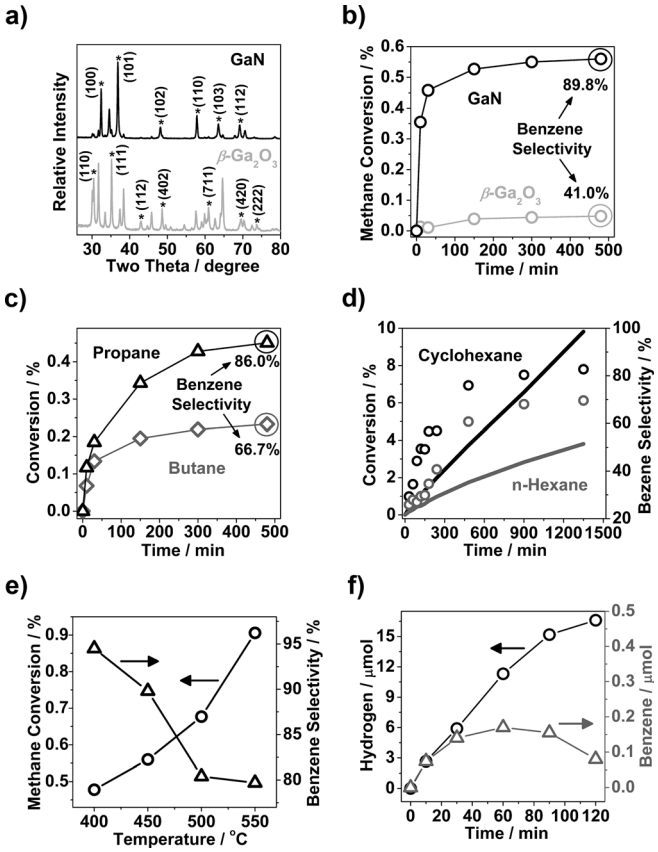

Figure 2. a) Powder X-ray diffraction patterns of GaN and Ga_2O_3. b) Methane conversion as a function of time over GaN and Ga_2O_3 at 450 °C. c) Propane and butane conversions as a function of time over GaN at 450 °C. d) Time courses of cyclohexane and *n*-hexane conversions (lines) with corresponding benzene selectivity (circles) over GaN at 450 °C. e) Plots of the methane conversion and benzene selectivity over GaN in 4 h as a function of the reaction temperature. f) Produced hydrogen and benzene as a function of time over GaN at 700 °C. Reaction conditions were as follows: catalyst, 20 mg; reactant, 100 μmol.

Brunauer-Emmett-Teller (BET) surface area of the GaN powders is 6.73 $m^2 g^{-1}$.

To begin our research, the catalytic performance of GaN for the conversion of light alkanes was tested at 450 °C in an airtight quartz reactor. After the reaction, the organic products were analyzed by jointly using gas chromatography and gas chromatography/mass spectrometry. To evaluate the different catalytic behaviors between gallium oxide and nitride, the same amount of β-Ga_2O_3 catalyst was prepared and used as the reference (Figure 2a). It was found that the nondoped GaN powders showed remarkable aromatization ability for all examined alkanes (methane, propane butane, *n*-hexane, and cyclohexane). The reaction led to the formation of benzene and hydrogen as the major products together with small amounts of other unsaturated hydrocarbons such as cyclohexene and toluene. Specifically, for methane conversion, besides benzene, the major organic by-products detected were cyclohexane (1.1%), toluene (3.0%), and a mixture of short-chain hydrocarbons less than C_6 (6.1%). Coke formation was found to be negligible at this temperature and few carbon oxides were detected by gas chromatography. Because of the thermodynamic intrinsic barrier of this reaction, a maximum methane conversion of 0.56% would be quickly achieved in 4 hours. In comparison, Ga_2O_3 gave a much lower methane conversion rate with a poor selectivity towards benzene (41.0%) under the same reaction conditions (Figure 2b). In the case of propane and butane, commonly referred to as natural liquified petroleum gas (Figure 2c), GaN also showed substantial activity for the non-oxidative dehydroaromatization reaction with good benzene selectivity (86.0% and 66.7% for propane and butane, respectively). The major by-product for either propane or butane is methane, which is generated from the carbon-chain cleavage. In the case of cyclohexane and *n*-hexane, a much higher conversion rate can be achieved since the intramolecular dehydroaromatization reaction is much more effective than the intermolecular ones (methane, propane, and butane). After a 24 hour reaction, a cyclohexane conversion of 9.8% with a benzene selectivity of 82.7% was achieved over GaN, and no induction period was observed at the initial stage. For comparison, a lower cyclohexane conversion (5.82%) with lower benzene selectivity (57.0%) was obtained over Ga_2O_3 under the identical reaction conditions. It is also noted that the benzene selectivity for either *n*-hexane or cyclohexane increased gradually with extending reaction time, since the transformation of light alkanes under such non-oxidative conditions are thermodynamically more favorable for benzene than to other olefins (see Figure S2 in the Supporting Information). The effect of temperature on methane con-

 © 2014 Wiley-VCH Verlag GmbH & Co. KGaA, Weinheim

version over GaN is also depicted in Figure 2e. The catalytic results obtained after a 4 hour reaction indicated that increasing the temperature from 400 to 550 °C enhanced the conversion of methane but slightly decreased the selectivity of benzene. The methane conversion reactions were also carried out at higher temperature. At 600 °C, a methane conversion of about 2.0 % can be achieved within 2 hours. In the case of 700 °C, a methane conversion of about 8.3 % can be achieved within 2 hours. However, as shown in Figure 2f, a further dehydrogenation of benzene to form polycyclic aromatic derivatives and carbon deposits became dramatic at 700 °C if the produced benzene was not removed from the reactor promptly.

The reusability of GaN for methane conversion was tested at 450 °C (Figure 3a). The results showed that the GaN catalyst can be used repeatedly without noticeable deactivation after ten catalytic runs. The crystal structure of the catalyst sample remained intact after reaction run for a long

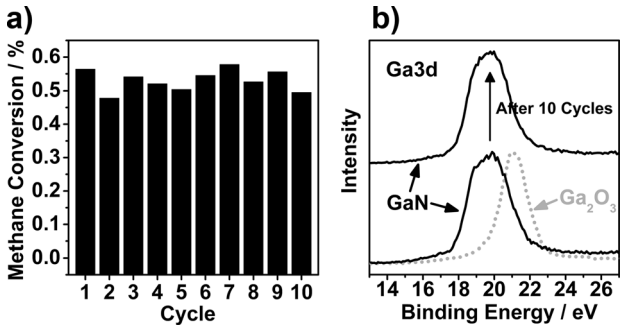

Figure 3. a) Reusability of GaN for the methane dehydroaromatization reaction at 450 °C (4 h for each cycle). b) XPS spectra of $Ga3d_{5/2}$ for the Ga_2O_3 (dotted curve) and GaN sample before (lower solid curve) and after (upper solid curve) ten cycles of the methane aromatization reaction.

time, as judged by the powder X-ray diffraction. As shown in Figure 3b, the X-ray photoelectron spectroscopy (XPS) spectra of Ga3d in GaN and Ga_2O_3 are centered at 19.7 and 21.1 eV, respectively, thus corresponding to Ga–N bonds and Ga–O bonds.[25] The XPS spectrum for the GaN powders after ten catalytic cycles was essentially the same as that for the fresh GaN. Neither of the binding energy peaks with maxima at 19.1 (typical for Ga^+) nor 17.7 eV (typical for Ga^0) was detected, and the only gallium signal in the XPS spectrum corresponds to Ga^{3+} species.[26] These results combined with the previous observation of the absence of an induction period, clearly demonstrate that the GaN material is chemically stable for the methane conversion reaction at high temperature for a long time and its lattice Ga^{3+} cations were not reduced to additional active centers during the reaction.

To gain further insight into the role of GaN at the molecular level, CH_4 adsorption process on the surface of GaN was studied using density functional theory (DFT) calculations. Our previous experimental studies under photolytic conditions have shown that the catalytic performance of GaN materials for the methane C–H bond activation is surface sensitive and depends strongly on the exposed *m*-plane but is not correlated with the *c*-plane.[22] However, the interaction mechanism between methane and the GaN *m*-plane is still not clear. The surface lattice of the GaN *m*-plane is composed of alternating Ga^{3+} and N^{3-} ions, which can produce strong local electrostatic polarization along the *c*-direction and thus, stretch and weaken the absorbed methane. In principle, two alternative adsorption models can be proposed. The first alkyl ($C^{\delta-}$–$H^{\delta+}$) model considers the methyl part of methane interacting with Ga to form a Ga/methyl species, whereas in the second carbenium model ($C^{\delta+}$–$H^{\delta-}$) the H atoms of methane are bounded to Ga to form Ga hydride species. Unable to determine adsorption configuration experimentally, we resulted to DFT calculations to get the optimized geometries for the two types of adsorption models mentioned above. Figure 4a and Figure S3 (see the

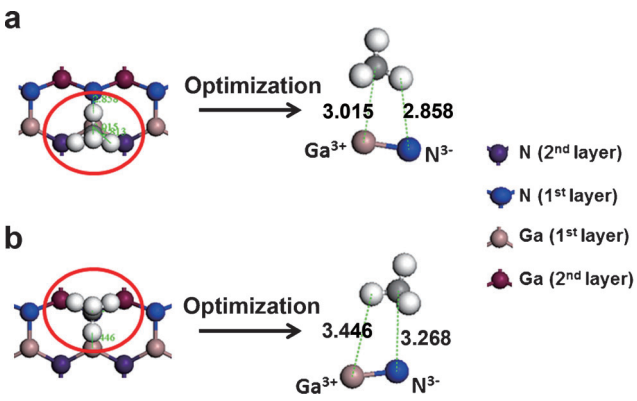

Figure 4. a) The alkyl and b) carbenium adsorption models between methane and the *m*-plane of GaN optimized by using DFT calculations. Bond lengths are in Å. White H, gray C.

Supporting Information) provide the most stable adsorption configuration for the methane molecule on the exposed *m*-plane of GaN through the alkyl adsorption way. The key feature of this structure is that the carbon atom in methane is attracted by the lattice Ga^{3+} cation, wherein one hydrogen atom in methane is absorbed by the surrounded lattice N^{3-} anion, and the other three hydrogen atoms are situated on the opposite side. In the case of carbenium model (Figure 4b), no stable adsorption configuration was found for methane on the surface of GaN: the methane molecule was pushed away after geometry optimization when H and C atoms were placed close to the lattice Ga and N, respectively. Our calculation results imply that the alkyl interaction way is energetically more favorable that the carbenium one. Interestingly, a similar interaction between methane and Ga-modified oxides has been observed by others through using in situ ^{13}C solid-state NMR spectroscopy, which partially supported our proposed interaction mechanism.[27]

Additionally, we calcined the GaN sample in air at 550 °C for 5 hours, and then tested the methane aromatization reactions under the same reaction conditions described above. During the calcination treatment, the structure of GaN remained intact but a thin layer of oxygen was produced on the surface of GaN (see Figure S4 in the Supporting Information). As a result, the catalytic activity decreased by

© 2014 Wiley-VCH Verlag GmbH & Co. KGaA, Weinheim

3.2-fold compared with the intact one, thus further indicating that GaN is the active species for the methane dehyroaromatization reaction and a trace amount of GaO_x impurities which may exist on the surface of GaN powders have negligible contributions to the catalytic activity.

In summary, an efficient and cost-effective metal nitride thermal catalyst for the non-oxidative dehydroaromatization of light alkanes has been discovered for the first time. Compared with gallium oxides, GaN catalysts exhibit both superior activity and selectivity towards benzene for all examined light alkanes, from methane to *n*-hexane. Further optimization of the reaction in term of increasing the methane covnersion and minimizing coke deposits at much higher temperature under flow conditions (> 700 °C) is in progress.

Experimental Section

Catalytic test: All the tests were performed under dry Ar atmosphere or vacuum using Schlenk glassware, glove box or vacuum line techniques. All the gaseous reactants were dried by passing the corresponding gases through a column of $MgSO_4$ and $CuSO_4$ prior to catalytic testing. The GaN and Ga_2O_3 powders used in this study were purchased from Sigma–Aldrich Company. The activity for the thermal-driven light alkane conversion reaction was evaluated in an airtight quartz reactor (75 cm^3) at 450 °C. 20 mg of the solid material was spread evenly at the bottom of the closed quartz reactor, and then evacuated at 550 °C for 2 h to remove the water and other molecules adsorbed in/on the solid material. Afterwards, the reactor was cooled slowly to 450 °C under vacuum ($P < 1$ Pa), followed by reaction with 100 μmol of the corresponding light alkane. During the reactions, the organic reactants and products were in-situ analyzed by jointly using gas chromatography (GC) with a flame ionization detector (FID) and gas chromatography-mass spectrometry. The amounts of carbon oxides or hydrogen (if any) were directly measured by GC with a thermal conductivity detector (TCD). For the recycling test, after each cycle, the catalytic system was evaluated again at 550 °C for 1 h to completely remove all the reactants and products molecules adsorbed in/on the solid material. Afterwards, the reactor was cooled back to 450 °C under vacuum ($P < 1$ Pa), followed by the injection of 100 μmol of corresponding fresh light alkane.

General characterization: The powder X-ray diffraction (XRD) patterns were recorded on a Bruker D8 Advanced Diffractometer with Cu Kα radiation ($\lambda = 1.5418$ Å). High resolution bright field transmission electron microscope (TEM) images were obtained using FEI Tecnai G2 F20 S/TEM at accelerating voltage of 200 kV. The X-ray photoelectron spectroscopy (XPS) was performed on an ESCALAB 250 X-ray photoelectron spectrometer with a monochromated X-ray source (Al Kα $h\nu = 1486.6$ eV). The energy scale of the spectrometer was calibrated using $Au4f_{7/2}$, $Cu2p_{3/2}$, and $Ag3d_{5/2}$ peak positions. The standard deviation for the binding energy (BE) values was 0.1 eV. The Brunauer-Emmett-Teller (BET) surface area of the sample was measured from the adsorption of N_2 at 77.4 K by using a Micromeritics TriStar 3000 system.

Received: September 2, 2014
Published online: October 21, 2014

Keywords: alkanes · C—H activation · density functional calculations · gallium · heterogeneous catalysis

[1] M. Guisnet, N. S. Gnep, *Appl. Catal. A* **1992**, *89*, 1 – 30.
[2] J. H. Lunsford, *Catal. Today* **2000**, *63*, 165 – 174.
[3] F. Solymosi, A. Széchenyi, *J. Catal.* **2004**, *223*, 221 – 231.
[4] A. Holmen, *Catal. Today* **2009**, *142*, 2 – 8.
[5] A. A. Gabrienko, S. S. Arzumanov, D. Freude, A. G. Stepanov, *J. Phys. Chem. C* **2010**, *107*, 8355 – 8362.
[6] H. Schwarz, *Angew. Chem. Int. Ed.* **2011**, *50*, 10096 – 10115; *Angew. Chem.* **2011**, *123*, 10276 – 10297.
[7] J. J. Spivey, G. Hutchings, *Chem. Soc. Rev.* **2014**, *43*, 792 – 803.
[8] a) L. Wang, L. Tao, M. Xie, G. Xu, *Catal. Lett.* **1993**, *21*, 35 – 41; b) D. J. Wang, J. H. Lunsford, M. P. Rosynek, *J. Catal.* **1997**, *169*, 347 – 358; c) H. Zheng, D. Ma, X. H. Bao, J. Z. Hu, J. H. Kwak, Y. Wang, C. H. F. Peden, *J. Am. Chem. Soc.* **2008**, *130*, 3722 – 3723.
[9] M. V. Luzgin, V. A. Rogov, S. S. Arzumanov, A. V. Toktarev, A. G. Stepanov, V. N. Parmon, *Angew. Chem. Int. Ed.* **2008**, *47*, 4559 – 4562; *Angew. Chem.* **2008**, *120*, 4635 – 4638.
[10] L. Wang, R. Ohnishi, M. Ichikawa, *J. Catal.* **2000**, *190*, 276 – 283.
[11] L. Li, G. D. Li, C. Yan, X. Y. Mu, X. L. Pan, X. X. Zou, K. X. Wang, J. S. Chen, *Angew. Chem. Int. Ed.* **2011**, *50*, 8299 – 8303; *Angew. Chem.* **2011**, *123*, 8449 – 8453.
[12] R. Ahuja, B. Punji, M. Findlater, C. Supplee, W. Schinski, M. Brookhart, A. S. Goldman, *Nat. Chem.* **2010**, *3*, 167 – 171.
[13] X. Guo, G. Fang, G. Li, H. Ma, H. Fan, L. Yu, C. Ma, X. Wu, D. Deng, M. Wei, D. Tan, R. Si, S. Zhang, J. Li, L. Sun, Z. Tang, X. Pan, X. Bao, *Science* **2014**, *344*, 616 – 619.
[14] V. R. Choudhary, A. K. Kinage, T. V. Choudhary, *Science* **1997**, *275*, 1286 – 1288.
[15] R. Fricke, H. Kosslick, G. Lischke, M. Richter, *Chem. Rev.* **2000**, *100*, 2303 – 2405.
[16] B. Liu, Y. Yang, A. Sayari, *Appl. Catal. A* **2001**, *214*, 95 – 102.
[17] N. Rane, A. R. Overweg, V. B. Kazansky, R. A. van Santen, E. J. M. Hensen, *J. Catal.* **2006**, *239*, 478 – 485.
[18] L. Li, Y. Y. Cai, G. D. Li, X. Y. Mu, K. X. Wang, J. S. Chen, *Angew. Chem. Int. Ed.* **2012**, *51*, 4702 – 4706; *Angew. Chem.* **2012**, *124*, 4780 – 4784.
[19] K. Shimizu, A. Satsuma, T. Hattori, *Appl. Catal. B* **1998**, *16*, 319 – 326.
[20] G. L. Price, V. Kanazirev, *J. Catal.* **1990**, *126*, 267 – 278.
[21] J. S. J. Hargreaves, *Coord. Chem. Rev.* **2013**, *257*, 2015 – 2031.
[22] L. Li, S. Z. Fan, X. Y. Mu, Z. Mi, C.-J. Li, *J. Am. Chem. Soc.* **2014**, *136*, 7793 – 7796.
[23] H. P. T. Nguyen, S. Zhang, K. Cui, X. Han, S. Fathololoumi, M. Couillard, G. A. Botton, Z. Mi, *Nano Lett.* **2011**, *11*, 1919 – 1924.
[24] O. Ambacher, M. S. Brandt, R. Dimitrov, T. Metzger, M. Stutzmann, R. A. Fischer, A. Miehr, A. Bergmaier, G. Dollinger, *J. Vac. Sci. Technol. B* **1996**, *14*, 3532 – 3542.
[25] S. D. Wolter, B. P. Luther, D. L. Waltemyer, C. Önneby, S. E. Mohney, R. J. Molnar, *Appl. Phys. Lett.* **1997**, *70*, 2156 – 2158.
[26] A. I. Serykh, M. D. Amiridis, *Surf. Sci.* **2009**, *603*, 2037 – 2041.
[27] M. V. Luzgin, A. A. Gabrienko, V. A. Rogov, A. V. Toktarev, V. N. Parmon, A. G. Stepanov, *J. Phys. Chem. C* **2010**, *114*, 21555 – 21561.

© 2014 Wiley-VCH Verlag GmbH & Co. KGaA, Weinheim